Development and Validation of an MRI-Derived Head-Neck Finite Element Model

Hossein Bahreinizad[1], Suman Chowdhury[1*], Leonardo Wei[1], Gustavo Paulon[1], Felipe Z. Santos[1]

[1]Department of Industrial, Manufacturing and Systems Engineering, Texas Tech University, Lubbock, Texas, USA

Running head: A Novel Head-Neck Finite Element Model

*All correspondence should be addressed to—

Dr. Suman Chowdhury, Assistant Professor, Department of Industrial, Manufacturing and Systems Engineering, Texas Tech University

905 Canton Ave, Lubbock 79409-3061, Texas, USA.

. E-mail: suman.chowdhury@ttu.edu; Tel: +1-806-834-7908.

Abstract

This study aimed to develop a biofidel head-neck FE model comprised of scalp, skull, CSF, brain, dura mater, pia mater, cervical vertebrae and discs, 14 ligaments, and 42 neck muscles. We assessed the geometrical accuracies of all model structures. The model was validated by replicating three experimental studies: NBDL's high acceleration profile, Zhang's linear and rotational acceleration profiles, and Nahum's impact study. The results showed reasonable geometrical fidelity. The intracranial pressure and brain stress data of our head-only model (excluded neck structures and constrained the base of the skull) were similar to Nahum's and Zhang's reported results. As neck structures were not considered in Nahum's and Zhang's studies, the FE results of our head-neck model showed slight discrepancies. Notably, the addition of neck structures (head-neck model) reduced brain stress-strain values and uncovered the brain's intracranial pressure dynamics, which the head-only model failed to capture. Nevertheless, the FE simulation results showed a good agreement ($r > 0.97$) between the kinematic responses of our head-neck model and NBDL's experimental results. Therefore, the developed head-neck model can be used as a computational tool for an accurate and comprehensive understanding of the brain injury mechanism in various head impact scenarios.

Keywords – Finite element method, Head-neck biomechanics, Brain injury, Computational biomechanics, MRI-driven modeling.

ABBREVIATIONS

CSF	Cerebrospinal fluid
CT	Computed tomography
FE	Finite element
MRI	Magnetic resonance imaging
NBDL	Naval biodynamics laboratory
PCSA	physiological cross-section area
SD	Standard deviation
3-D	Three dimensional

Introduction

Throughout history, computational head-neck models based on finite element (FE) methods have been used to assess the biomechanical responses of the brain and other head-neck components for various head impact scenarios, commonly seen in contact sports[35], motor vehicle accidents[39], battlefields[54], and occupational settings[52]. This is because FE modeling is obvious to understand if the spatial and temporal distributions of the stress waves following a head impact exceed the strength and deformation tolerance limits of the constituent structures – which are otherwise difficult to measure using in-vivo experiments. However, the accuracy of these head-neck FE models depends on accurate geometric and material characterizations of biological tissues and their inter-structural biomechanical interactions. With the recent advancement in computational power and the availability of tissue material properties, modeling the complex geometries of the head-neck structures has become a lesser challenging task than ever. Yet, despite this progress, there has been a lack of effort to develop a sophisticated and biofidel (biologically more accurate) head-neck FE model.

The computational modeling of head-neck structures remains challenging due mainly to the large variability in their mechanical properties. For instance, scalp exhibited high damping characteristics and linear elastic behavior under mechanical loads[42]. Skull showed a linear viscoelastic behavior with a higher stiffness in the elastic region[15]. The brain tissue displayed an anisotropic, non-linear viscoelastic behavior because of its' high water content[9]. In contrast, modeling the fluid behavior of cerebrospinal fluid (CSF) requires CSF-skull and CSF-brain interfaces to be defined as complex fluid-structure interfaces. That was why most previous studies had modeled CSF as a linear or nonlinear solid material with low stiffness, high bulk modulus, and high Poisson's ratio to mimic its' fluid-like behavior[17] and its' interactions with other tissues as tied or sliding contacts[17, 25]. Similarly, to reduce additional complexities in the FE modeling and simulation process, the interactions between other head-neck substructures were also modeled as tied and/or sliding contact interfaces. On the other hand, neck structures were found to play an essential role in the brain injury mechanism[4]. For instances, cervical intervertebral discs dampen the impact waves[30], and neck muscles reduce undesirable head-neck kinematics during dynamic impact simulations[8]. As such, cervical discs were modeled as hyper-viscoelastic materials[26], cervical bones as linear elastic materials[26], and ligaments as one-dimensional springs[56]. In contrast, the tetanized muscle contraction was primarily modeled with Hill's muscle model[11, 50], consisting of non-linear active (contractile) and passive elements.

Besides material properties, the accuracy in geometry generation and the choice of FE meshing method (mesh type, element size, and mesh quality) are crucial to ensure that the head-neck models provide accurate numerical solutions[18, 33]. This becomes even more critical when developing a detailed head-neck model because coupling many inaccurate surfaces in a complex model leads to singularities and divergence[18]. Similarly, an inappropriate meshing of a biological structure, even for geometrically accurate

structures, was found to yield misleading numerical results[1, 18]. Particularly, finer meshes are required in critical areas, such as contact interfaces, high-stress gradient areas, and other critical regions of interest[53]. For example, some previous studies modeled skull, brain, and CSF[21, 24] with coarse meshes and hexahedral elements to run their models with available computing power; however, they sacrificed important anatomical details of head structures (such as brain sulci and gyri structure or finer details of the cranium surface). Thereby, they failed to capture comprehensive details of the head responses. On the contrary, recent advancements in computing technology enabled researchers to generate high-quality finer meshes to represent those complex anatomical details[17, 23, 26]. Nonetheless, a finer mesh can be time-consuming. Therefore, it is essential to define the optimized mesh size that provides time-effective simulations while, at the same time, do not compromise real-world anatomical fidelity.

Despite these challenges, many computational FE models have been developed over the years to investigate the causation and effectuation of head and brain injuries in various impact scenarios. These models differ greatly in anatomical details, ranging from low to high fidelity[26, 31, 34] and from geometrically and mechanically simplistic[37] to complex[26] descriptions of various head-neck structures. Early head FE models were developed in 1970s[37, 49] wherein researchers used linear elastic material properties and simplified geometries to represent complex head tissues so that they could be solved with available, limited computational power. As more material properties and computing power gradually became available, many researchers attempted to add complexities to their head models. Particularly, some studies attempted to include various neck structures, such as cervical vertebra[43], cervical discs[45], and neck muscles and ligaments[26] in their head models. As modeling these head-neck structures with their detailed geometric and mechanical characterizations is a time-, labor-, and technology-intensive challenging task, only a handful of researchers have attempted to create complete, sophisticated head-neck FE models. Notably, the global human body model consortium[16] and Total Human Model for Safety[21] models were developed to study head impact biomechanics in motor vehicle accidents. Although these models included many head-neck anatomical features, their two significant limitations are coarse meshing and simplistic geometry of complex head-neck structures. Recently, Tse et al.[44] and Tuchtana et al.[45] also proposed head-neck FE models without active neck muscles. On the contrary, two recent studies included active neck muscles in their head-neck FE models[3, 26]. For instance, Liang et al.[26] developed a head-neck model with active neck muscles; however, this model did not include any CSF. Barker et al.[3] also proposed a head-neck model with active muscles; however, they did not include brain in their model.

Furthermore, the advancement in medical imaging techniques, such as computed tomography (CT) and magnetic resonance imaging (MRI), has contributed to the development of a biofidel head-neck model. CT imaging and MRI scans are traditionally used to capture hard (e.g., vertebrae, skull, etc.) and soft tissues (e.g., muscles, ligaments, etc.), respectively. Some previous studies have used both CT and MRI techniques to image the irregular shapes of head and neck structures[26]. Nonetheless, it

could be cumbersome to avoid alignment issues between CT and MRI images during the 3-D model development stage. In addition, CT imaging exposes human subjects to harmful radiation[41], whereas MRI uses strong magnetic fields to capture the tissues of interest without any ionizing radiation. Though MRI scanning is traditionally implemented to image soft tissues, the recent development of MRI techniques[28] has unlocked the door for high-quality imaging of both soft and hard tissues. To our knowledge, three previous studies[6, 17, 23] have exclusively used MRI datasets to develop a head FE model; however, none of them considered any neck structures. Therefore, this study aimed to develop an MRI-based biofidel head-neck FE model and validate its' anatomical accuracy and biomechanical performance by using experimental data.

Materials and Methods

MRI-derived head-neck FE model development

The methodological framework of our head-neck FE model development procedures is presented in Figure 1. We used head and neck MRI datasets of a male participant (age: 42 years, height: 176 cm, and weight: 106 kg) throughout the whole modeling procedure. Prior to the MRI procedure, we collected written informed consent from the subject. The study protocol was approved by the local institutional review board (*IRB 2020-708*).

Head-neck geometry development

We obtained high-quality hard and soft tissue images of head-neck structures ranging from the top of the scalp to the third thoracic vertebra by implementing T-1 weighted and T-2 weighted sequences at a 3T MRI scanner (Siemens Medical Solution, Germany). T2-weighted images were primarily used since this sequence employed different gray values to distinguish soft and hard tissues and fluids more accurately. Then, we generated high-fidelity anatomical features of scalp, skull, brain, pia matter, dura matter, CSF, cervical bones (C1-C7), and intervertebral discs by processing their MRI images in MIMICS 24.0 and 3-Matic 16.0 software platforms (both from Materialise Inc., Belgium). The MRI data were re-sliced at every 0.5 mm to enhance soft-hard tissue contrast in the neck region. Subsequently, we segmented MRI images of each head-neck structure of interest via identifiable masks and created their 3-D geometry in MIMICS. Then, we exported 3-D point clouds of each geometry into the 3-Matic platform to remove noises and unwanted tissues that were not entirely removed in MIMICS (Fig. 1).

*** Insert FIGURE 1 here***

FIGURE 1. A schematic presentation of the methodological framework. The framework follows four consecutive steps: 1) 3-D head-neck geometry development from MRI datasets, 2) Geometrical verification of developed images, 3) FE meshing of the model geometries, and 4) defining material properties. Steps to generate and verify head-neck

geometry are shown in the top dashed box, and the steps for the finite element modeling are provided in the bottom dashed box.

Head-neck geometry verification

Once the 3-D geometries of all head-neck structures were created, we verified the accuracies of their individual geometrical parameters (e.g., shape, size, and volume) and alignments with the literature data. Their geometrical parameters were determined by following steps as described in previous studies[2, 12, 19, 20, 47]. For example, the *minimum scalp thickness* was automatically calculated in ANSA (BETA CAE Systems SA, Greece) software, whereas the *maximum scalp thickness* was chosen as the highest thickness value among the values manually measured at frontal, temporal, occipital, and parietal lobes[20]. The average *skull thickness* was measured in six cranium sites (F3, F4, T3, T4, P3, P4) as specified by Hagemann et al.[20]. *Brain and CSF volumes* were also measured automatically in ANSA software. The geometries of neck vertebral bodies and discs were measured by identifying four corner-most points (anterior-superior, anterior-inferior, posterior-superior, posterior-inferior points) of the vertebral body and two corner-most points (distal and proximal ends) of their spinous process in the mid-sagittal plane as described in the literature[47]. The *vertebral height* was the average of anterior (distance from anterior-superior to anterior-inferior points) and posterior (distance from posterior-superior to posterior-inferior points) body heights, the *vertebral depth* was the average of superior (distance from posterior-superior to anterior-superior points) and inferior (distance from anterior-inferior to posterior-inferior points) vertebral body widths, *spinous process length* was the distance between distal and proximal corner-most points of the spinous process, and the *vertebral body to spinous process length* was the distance between the distal end of the spinous process and posterior side of the vertebrae body. Furthermore, we calculated angle-corrected *disc heights* as described in litreature[14].

During the MRI procedure, the subject was required to lie flat and use pillows to immobilize his head and neck, which might have led to some degrees of neck tilt. Thence, we examined the orientation of each neck vertebral body with respect to a neutral, upright neck orientation. We employed principal component analysis to calculate principal components and the centroid of each vertebral body in MATLAB R2021b (MathWorks, USA) platform. Then, we rotated each vertebral body with regard to its own centroid and matched its' first three principal components with the global coordinates of the model. Furthermore, we rotated and translated C2, C3, C4, C5, C6, and C7 vertebrae to match the frontal and sagittal planes of the C1 vertebra.

Mesh generation and model assembly

We used the ANSA platform to generate high-fidelity finer meshes of all head-neck structures. To maintain the quality of the mesh structure, we used 3, 45, 10, and 0.7 as threshold values for aspect ratio, skewness, warping, and max angle, respectively. The meshing process continued for a given structure until it met the target mesh quality criteria. The resulting meshed model included 1.82 million tetrahedral elements, in which

scalp, skull, CSF, brain, and neck have 0.27, 0.47, 0.33, 0.68, and 0.072 million elements, respectively, and 0.081 million triangular shell elements wherein dura and pia maters have 0.02 and 0.06 million elements (Fig. 2).

Furthermore, we included 21 muscles on both the left and right sides of the neck and 14 ligaments around the neck. We modeled the ligaments as linear springs with 486 beam elements, and their stiffness was adopted from litreature[56]. Similarly, neck muscles were also modeled as beam elements, with a total of 132 elements. The origin and insertion points of these muscles and ligaments were adopted from Gray's anatomy book[38].

*** Insert FIGURE 2 here***

FIGURE 2. A schematic presentation of our developed head-neck finite element model consisting of scalp, skull, brain, CSF, pia mater, dura mater, cervical vertebrae (C1-C7), intervertebral discs, muscles (obliquus capitis superior, superior longus colli, rectus capitus major, rectus capitus minor, longus capitis, rectus capitis ant, rectus capitis lat, anterior scalene, middle scalene, posterior scalene, sternocleidomastoid, longissimus capitis, longissimus cervicis, multifidus cervicis, semisplenius capitus, semispinalis cervicis, splenius capitis, splenius cervicis, levator scapula, oblique capitus inferior and trapezius), and ligaments (anterior longitudinal ligament, posterior longitudinal ligament, ligamentum flavum, capsular ligament, interspinous ligaments, tectorial membrane, anterior and posterior atlanto-occipital ligaments, anterior and posterior atlanto-axial ligaments, apical ligament, alars ligament, transverse ligament, and cruciate ligament of atlas).

Defining material properties and model assembly

The material properties and governing equations of all head-neck structures included in our model are provided in Table 1. Briefly, we modeled skull, pia mater, dura mater, and vertebrae as linear elastic material[36, 43, 45], scalp as a linear viscoelastic material model[27], CSF as nearly incompressible one-term hyper-elastic material[7], intervertebral discs as a hyper-viscoelastic material model[5], and brain as a hyper-viscoelastic material[13]. As the scalp shows load-rate-dependent mechanical characteristic[42] and has very low stiffness, it is expected to rupture under high-impact loads. Therefore, we applied the erosion model available in the LS-DYNA (Livermore Software Technology Corporation, USA) platform to identify and remove ruptured tissues if the strain of any scalp element exceeded 60%[22].

*** Insert Table 1 here***

Moreover, we modeled the muscles using the hill-type muscle model. Muscle volume and physiological cross-section area (PCSA) were taken from the literature[30]. Muscle resting length was calculated as muscle volume divided by its' PCSA. The maximum velocity of a muscle was set to 10 times its resting length. The maximum stress of a muscle was set to 0.3 MPa[51].

Similar to previous studies[17, 27], we implemented tied boundary contact between discs and vertebrae, skull and scalp, Skull and dura mater, dura mater and CSF, CSF and pia mater, brain and pia mater and neck-skull articulations. Moreover, the bottom surface of the C7 cervical vertebra was fixed to restrict its' all degrees of freedom.

Experimental Data for head-neck FE model validation

Three head impact experiments[29, 40, 55] were used to validate the efficacy of our developed head-neck FE model (Fig. 3). Our first experimental dataset was the translational (Fig. 3a) and rotational (Fig. 3b) acceleration profiles of Zhang et al.[55] study. We numerically replicated them in two separate FE models: 1) head-only model, similar to the original numerical simulation, by constraining the base of the skull (the area around the foramen magnum) and 2) head-neck model to understand how the neck contributed to the mechanical responses of the head structures. The second experimental dataset was the linear acceleration profile (Fig. 3c) of an in-vivo study conducted by the Naval biodynamics laboratory (NBDL)[10] in 1973. Thunnissen et al.[40] corrected NBDL's linear acceleration profile for T1 vertebral rotation in 1995. We applied one of those corrected acceleration profiles[40] (Fig. 3c) to our head-neck model. As the subject's neck muscles were pre-tensed in the NBDL experiment, we modeled the flexor muscles with 0% activation and the extensor muscles with 80% activation. Our third experimental dataset was the impact study conducted by Nahum et al.[29], in which they analyzed the mechanical response (intracranial pressure) of the head of a cadaver subject. Similar to their experimental condition, we simulated a rigid aluminum impactor with a mass of 5.59 kg and a velocity of 9.94 m/s blowing the frontal bone of the skull in the direction of mid-sagittal plane, while the head was tilted 45° downward towards the ground (Fig. 3d). We meshed the impactor with 174,596 tetrahedral elements. The impact pulse lasted for about 5 ms, with a peak impact force of 10.76 kN at around 2.5 ms. We replicated Nahum's study for 1) head-only and 2) head-neck models to explore the differences in numerical solutions under the presence of neck structures. We used LS-DYNA explicit solver platform installed in the university high-performance computing center (with 128 CPU cores per node cluster) to solve all impact simulations.

*** Insert FIGURE 3 here***

FIGURE 3. Experimental impact scenarios that were numerically replicated in this study: a) three linear acceleration (A_x, A_y, A_z) and b) three rotational acceleration (R_x, R_y, R_z) profiles reconstructed by Zhang et al.[55] by analyzing twelve cases of helmet-to-helmet collisions occurred in American football using dummies, c) linear acceleration profile of Naval biodynamics laboratory (NBDL) study[10] with respect to T1 vertebral rotation[40], and d) Nahum et al.[29], in which they hit a cadaver head using rigid body impactor[29]. The run time for finite element simulations of Zhang et al.', NBDL,' and Nahum's studies were respectively 30 ms, 220 ms, and 8 ms.

Post-processing and statistical analysis

We used META (BETA CAE Systems SA, Greece) software for post-processing and retrieving numerical solutions of all three impact simulations. To compare with the actual numerical results of Zhang's study[55], we calculated overall intracranial pressure (positive and negative), local shear stress in the midbrain and thalamus regions, and the time of peak intracranial pressure (peak time) for both head-only and head-neck models. Similarly, we assessed intracranial pressure in frontal, parietal, and occipital lobes for both head-only and head-neck model simulations and compared our results against Nahum's impact results. Additionally, we compared the maximum principal strain of the brain at three impact instances to explore the contribution of neck structures on mechanical responses of the brain to Nahum's rigid body impacts. We also compared model-predicted neck flexion angle data and their peak time with the experimental neck flexion data of the NBDL study[40]. Pearson correlation analysis was employed for pairwise comparison between all numerical and experimental data patterns. For this purpose, we digitized Nahum's experimental intracranial pressure plots[29] and NBDL's experimental neck flexion angle plot[40] in the MATLAB platform. For the same digitized points, we retrieved model-predicted intracranial pressure data and neck positional information in the META platform. The neck flexion angle was the angle between the vertical line and the line joining the anterior-most point of the foramen magnum and the anterior-inferior corner-most point of C7 in the mid-sagittal plane.

Results

3-D head-neck geometry

The head geometry data exhibited that both skull thickness and brain volume of our model were within one standard deviation (SD) of the values reported in previous literature[12, 20] (Table 2). On the other hand, the model's CSF volume was found to be larger than the literature data[19] – about 6.75% greater than the maximum reported value. The maximum scalp thickness value was also observed to be 25.70% higher than the literature data[2].

*** Insert Table 2 here***

The neck geometry data showed that 16 out of 22 measures of cervical vertebra were observed to be within one SD of previously-reported values[47] (Table 3). Other six vertebral measurements (C3 height, C6 and C7 depth, C4 spinous process length, and C3 and C4 vertebral body to spinous process length) were within 17% of their corresponding reported values[47]. The disc height data also revealed that, except C5/C6 disc, all other discs were within one SD of the reported values[14] (Table 4).

*** Insert Table 3 here***

*** Insert Table 4 here***

FE simulation Results

We found a good agreement between our head-only model solutions and Zhang's numerical results[55]. The intracranial pressure (both positive and negative) and shear stress values of midbrain and thalamus in our head-only model were similar (within one SD range) to values reported by Zhang's study[55] (Table 5). The peak time in our head-only model was 10ms, which is very close to Zhang's reported peak time (9ms). In contrast, our head-neck model results exhibited a peak time at 24ms and a substantial reduction of shear stresses in midbrain (67.28%) and thalamus (47.31%) regions and positive (54.66%) and negative (57.17%) intracranial pressure values of the brain.

*** Insert Table 5 here***

The kinematic responses of our head-neck model duplicated the NBDL's experimental data very accurately. Our model showed a neck flexion angle of 36.98°±35.04°, with a peak of 88.80°, whereas the NBDL study reported 11 subjects' neck flexion angles, ranged between a mean angle of 39.69°~30.72° and the maximum angle of 67.20°~87.50°. Though a small number of discrepancies were found for the maximum neck angle (1.48% larger) and its' peak time (5 ms delay), the visual comparisons of kinematic behavior at three-time instances revealed analogous head-neck responses between model predictions and experimental simulations (Fig. 4). In addition, Pearson's correlation analysis evinced a strong positive correlation ($r > 0.97$) between experimental and numerical head-neck kinematic patterns (Fig. 4).

*** Insert Figure 4 here***

FIGURE 4. Comparison between model-predicted and NBDL-experimental neck flexion angles for the complete simulation duration (top) and a visual comparison between model-prediction (middle) and experimental head-neck kinematic responses (bottom) at three different time instances[40].

We also found a good agreement ($r = 0.80$~0.91) between model-predicted intracranial pressure data at frontal, parietal, and occipital regions for our head-only model and Nahum's experimental (cadaver head) results, except for minor differences (less than <10%) in peak intracranial pressure values. Nevertheless, the average intracranial pressure at frontal, parietal, and occipital regions were respectively 10.85%, 15.66%, and 18.45% lower for the head-only model than their corresponding experimental counterparts. On the contrary, the addition of neck structures led to 13.20%, 49.89%, and

27.38% decreased intracranial pressures at frontal, parietal, and occipital regions than their experimental counterparts (Table 5). The Pearson correlation analysis between head-neck model predictions and Nahum's experimental results also showed a low-to-medium level of correlation (r = 0.17 ~ 0.42) (Fig. 5). A visual representation of the impact scenarios in Fig.6 for three-time instances clearly revealed that the impactor was no longer in contact with the head in the head-only model in the last quarter (beyond 3.5 ms), whereas it was under impact in the head-neck model (at even 4.5 ms). Consequently, the occipital region in the head-neck model seemed to suffer a higher maximum principal strain (lighter blue) at 4.5 ms than the head-only model. Nevertheless, maximum principal strain values of the brain were comparatively lesser in the head-neck model than in the head-only model at both 0.5 ms and 4.5 ms.

*** Insert Figure 5 here***

FIGURE 5. Comparison between simulated intracranial pressure results and Nahum's experimental results[29] for both head-only (top) and head-neck (bottom) models at three different brain locations (frontal, parietal, and occipital). The correlation coefficients (r) are provided for each case.

*** Insert FIGURE 6 here***

FIGURE 6. The overall principal strain of the brain. The color map and corresponding values indicate the range of principal strain across all brain regions.

Discussion

In this study, we developed a biofidel head-neck FE model from MRI datasets and validated its' biomechanical responses against three experimental datasets[29, 40, 55]. The numerical solutions revealed that both head-only and head-neck models were capable of accurately simulating the experimental impact scenarios and predicted the biomechanical response of model structures (e.g., brain stress-strain tensor values) reasonably well. The present study also assessed the geometrical biofidelty of the head-neck model and found that the most geometrical measures other than scalp thickness, CSF volume, six vertebral body measures, and one disc measure were within the normal range of previously-reported values. Only scalp thickness and CSF volume were somewhat larger than their corresponding values in the literature[2, 19, 46]. In order to verify that they were not erroneously imaged and/or segmented in the T2 MRI sequence, we segmented T-1 weighted images of the same subject and found almost same scalp thickness and CSF

volume. Our study participant was a 92nd percentile male regarding weight[32], thus he might have a higher-than-average scalp thickness. In this study, we defined CSF volume as the space between the skull and brain, which includes dura and pia maters, intracranial blood vessels, meninges, etc. As we did not model other structures except dura and pia maters between the skull and brain, we conjecture that the inclusion of their spaces as CSF led to a larger CSF volume. Previous studies have also reported geometrical discrepancies in the neck region[3, 26, 47]. Such as, Liang et al.[26] observed larger C2 and C3 spinous process lengths, and Barker et al. [3] found higher posterior disc height than the reported literature data. This leads us to believe that, regardless of the imaging technique, voxel-based intensity standardization methods[48] should be implemented to enhance soft- and hard-tissue contrasts in the complex neck region. The lack of such an image processing method might have led to slight discrepancies in those six vertebral measures and one disc measure, even though we took utmost care to segment and reconstruct the 3D geometry of each head-neck structure.

When a mechanical impact is introduced to the head and neck system, the resultant movements (and/or stress) transfer(s) from one tissue to another and cause deformations in every head-neck structure. Therefore, it is crucial to ensure that our model was able to accurately reproduce these events and assess the mechanical behavior of all head-neck structures. For this purpose, we simulated three experimental studies: 1) Zhang's study[55] (high linear and rotational acceleration impacts that are common in contact sports), 2) NBDL study[40] (high linear acceleration impacts that are commonly seen in automotive and aviation accidents), and 3) Nahum's study (low-velocity projectile impacts[29] that are common in occupational and battlefield-related head traumas). The numerical results showed that the difference between model predictions and experimental data remained relatively small. For instance, our head-only model's parietal and occipital intracranial pressure values were very close to Nahum's experimental (cadaver head) results. Only a slight difference in the frontal intracranial pressure (9% lower) was observed due mainly to the extra thickness of the scalp that absorbed a greater amount of impact energy than usual. In addition, as delays in the mechanical response of a system are mainly caused by its damping characteristics, the addition of neck structures is expected to facilitate some delays in head-neck impact responses. For example, our simulation results of Zhang's study showed that the addition of neck structures (neck damping) caused a phase difference (14 ms) in the peak time of intracranial pressure between head-only and head-neck models. On the contrary, as we had also implemented some degrees of geometric and mechanical simplifications (e.g., linear elastic properties of bones) in our original model, slight differences between in-vivo results and our model predictions were expected. That being said, a high correlation ($r>0.97$) between neck flexion angle profiles and a slight difference (5 ms) in their peak time between NBDL experimental and numerical simulations suggested that the damping characteristics of our head-neck model were well-defined.

The addition of neck structures exhibited a substantial reduction in intracranial pressure, shear stress, and principal strain of the brain for both Nahum's study and

Zhang's study. As both of these studies did not consider neck structures, we expected discrepancies between our head-neck model predictions and their reported results. In the case of Nahum's study replication, we observed a sharp increase in intracranial pressure values at parietal and occipital lobes in the last quarter of the impact duration (Fig.5), for the reason that the already deformed neck structures (discs and extended neck muscles and ligaments) failed to attenuate additional impact energy from the impactor, which had already been bounced back in the head-only model (Fig. 6). This sudden increase in negative pressure at counter-coup locations (occipital and parietal regions) may cause the brain tissues and meninges to collapse. Like many previous head-only models, our head-only model had also failed to capture the roles played by the neck structures and thus led to an incomprehensive understanding of the intracranial pressure dynamics. Therefore, a FE model consisting of both head and neck structures is the most efficient and biofidel computational tool for an accurate and comprehensive understanding of brain and head injury mechanics for various (sub-) traumatic scenarios.

This study has several limitations. First, our entire brain model was defined as an orthotropic homogeneous material and was not separated into gray and white maters, which would uncover more inner workings of brain injury formation. Second, we simplified the model by considering identical, constant muscle activation for extension and flexor muscles which are different from brain-controlled actual muscle activation patterns. Third, we did not implement voxel-based intensity standardization in the image processing, leading to slight discrepancies in 3-D vertebral body geometries. Fourth, both skull and vertebral bodies were not separated into cancellous and cortical bones, and the CSF was not modeled as a pure fluid. Future works may make the model more biologically accurate by modeling cortical and cancellous bones separately and CSF as a fluid and CSF-skull and CSF-brain interfaces as fluid-structure interactions. Despite these limitations, our developed head-neck model was able to reproduce the experimental results accurately and provide valuable insights into the mechanical responses of the brain both without and under the presence of neck structures. In summary, our developed model took into account the neck damping characteristics, the scalp erosion model (to remove impact-induced ruptured tissues), and neck muscle mechanics. Therefore, the proposed head-neck model has the potential to be used as a computational tool for various applications, such as brain injury prediction, helmet design, motor vehicle safety, and ballistic head impact injury predictions.

Acknowledgments

Conflict of interest

The authors do not have any conflict of interest to declare.

References

1. Alañón A., E. Cerro-Prada, M. J. Vázquez-Gallo and A. P. Santos. Mesh size effect on finite-element modeling of blast-loaded reinforced concrete slab. *Engineering with Computers* 34: 649-658, 2018.
2. Babiloni F., C. Babiloni, F. Carducci, M. Del Gaudio, P. Onorati and A. Urbano. A high resolution EEG method based on the correction of the surface Laplacian estimate for the subject's variable scalp thickness. *Electroencephalography and clinical neurophysiology* 103: 486-492, 1997.
3. Barker J. B. and D. S. Cronin. Multilevel validation of a male neck finite element model with active musculature. *Journal of biomechanical engineering* 143: 2021.
4. Beusenberg M., N. Shewchenko, J. Newman, R. de Lange and H. Cappon. Head, neck, and body coupling in reconstructions of helmeted head impacts. *International Research Council on the Biomechanics of Impact, Isle of Man, UK* 295-310, 2001.
5. Castro A., C. Paul, S. Detiger, T. Smit, B. Van Royen, J. Pimenta Claro, M. Mullender and J. Alves. Long-term creep behavior of the intervertebral disk: comparison between bioreactor data and numerical results. *Frontiers in bioengineering and biotechnology* 2: 56, 2014.
6. Chen Y. and M. Ostoja-Starzewski. MRI-based finite element modeling of head trauma: spherically focusing shear waves. *Acta mechanica* 213: 155-167, 2010.
7. Cotton R., C. W. Pearce, P. G. Young, N. Kota, A. Leung, A. Bagchi and S. Qidwai. Development of a geometrically accurate and adaptable finite element head model for impact simulation: the Naval Research Laboratory–Simpleware Head Model. *Computer methods in biomechanics and biomedical engineering* 19: 101-113, 2016.
8. Eckner J. T., Y. K. Oh, M. S. Joshi, J. K. Richardson and J. A. Ashton-Miller. Effect of neck muscle strength and anticipatory cervical muscle activation on the kinematic response of the head to impulsive loads. *The American journal of sports medicine* 42: 566-576, 2014.
9. Eskandari F., M. Shafieian, M. M. Aghdam and K. Laksari. Structural anisotropy vs. mechanical anisotropy: the contribution of axonal fibers to the material properties of brain white matter. *Annals of biomedical engineering* 49: 991-999, 2021.
10. Ewing C. L. and D. J. Thomas. Human Head and Neck Response to Impact Acceleration. Naval Aerospace Medical RESEARCH Lab Pensacola Fl, 1972.
11. Fice J. B., D. S. Cronin and M. B. Panzer. Cervical spine model to predict capsular ligament response in rear impact. *Annals of Biomedical Engineering* 39: 2152-2162, 2011.
12. Filipek P. A., C. Richelme, D. N. Kennedy and V. S. Caviness Jr. The young adult human brain: an MRI-based morphometric analysis. *Cerebral cortex* 4: 344-360, 1994.
13. Fournely M., Y. Petit, E. Wagnac, M. Evin and P.-J. Arnoux. Effect of experimental, morphological and mechanical factors on the murine spinal cord subjected to transverse contusion: A finite element study. *PLoS One* 15: e0232975, 2020.
14. Frobin W., G. Leivseth, M. Biggemann and P. Brinckmann. Vertebral height, disc height, posteroanterior displacement and dens–atlas gap in the cervical spine: precision measurement protocol and normal data. *Clinical Biomechanics* 17: 423-431, 2002.
15. Fung Y.-c. *Biomechanics: mechanical properties of living tissues*. Springer Science & Business Media, 2013.

16. Gayzik F. S., C. A. Hamilton, J. C. Tan, C. McNally, S. M. Duma, K. D. Klinich and J. D. Stitzel. A multi-modality image data collection protocol for full body finite element model development. *SAE Technical Paper* 2261, 2009.
17. Ghajari M., P. J. Hellyer and D. J. Sharp. Computational modelling of traumatic brain injury predicts the location of chronic traumatic encephalopathy pathology. *Brain* 140: 333-343, 2017.
18. Giudice J. S., W. Zeng, T. Wu, A. Alshareef, D. F. Shedd and M. B. Panzer. An analytical review of the numerical methods used for finite element modeling of traumatic brain injury. *Annals of Biomedical Engineering* 47: 1855-1872, 2019.
19. Grant R., B. Condon, A. Lawrence, D. Hadley, J. Patterson, I. Bone and G. Teasdale. Human cranial CSF volumes measured by MRI: sex and age influences. *Magnetic resonance imaging* 5: 465-468, 1987.
20. Hagemann D., J. Hewig, C. Walter and E. Naumann. Skull thickness and magnitude of EEG alpha activity. *Clinical Neurophysiology* 119: 1271-1280, 2008.
21. Iwamoto M., Y. Kisanuki, I. Watanabe, K. Furusu, K. Miki and J. Hasegawa. Development of a finite element model of the total human model for safety (THUMS) and application to injury reconstruction. In: *Proceedings of the international IRCOBI Conference*2002, p. 18-20.
22. Jussila J., A. Leppäniemi, M. Paronen and E. Kulomäki. Ballistic skin simulant. *Forensic science international* 150: 63-71, 2005.
23. Khanuja T. and H. N. Unni. Intracranial pressure–based validation and analysis of traumatic brain injury using a new three-dimensional finite element human head model. *Proceedings of the Institution of Mechanical Engineers, Part H: Journal of engineering in medicine* 234: 3-15, 2020.
24. Kleiven S. Predictors for traumatic brain injuries evaluated through accident reconstructions. *Stapp car crash J* 51: 81-114, 2007.
25. Kleiven S. and W. N. Hardy. Correlation of an FE model of the human head with local brain motion: consequences for injury prediction. *Stapp car crash journal* 46: 123-144, 2002.
26. Liang Z., M. Fuhao, Z. Zheng, Y. Li, Y. Tian, X. Jiang and T. Liu. Quantitative cervical spine injury responses in whiplash loading with a numerical method of natural neural reflex consideration. *Computer Methods and Programs in Biomedicine* 219: 106761, 2022.
27. Mao H., L. Zhang, B. Jiang, V. V. Genthikatti, X. Jin, F. Zhu, R. Makwana, A. Gill, G. Jandir and A. Singh. Development of a finite element human head model partially validated with thirty five experimental cases. *Journal of biomechanical engineering* 135: 111002, 2013.
28. Mastrogiacomo S., W. Dou, J. A. Jansen and X. F. Walboomers. Magnetic resonance imaging of hard tissues and hard tissue engineered bio-substitutes. *Molecular imaging and biology* 21: 1003-1019, 2019.
29. Nahum A. M., R. Smith and C. C. Ward. Intracranial pressure dynamics during head impact. SAE Technical Paper, 1977.
30. Panzer M. B., J. B. Fice and D. S. Cronin. Cervical spine response in frontal crash. *Medical engineering & physics* 33: 1147-1159, 2011.

31. Panzer M. B., B. S. Myers, B. P. Capehart and C. R. Bass. Development of a finite element model for blast brain injury and the effects of CSF cavitation. *Annals of Biomedical Engineering* 40: 1530-1544, 2012.
32. Paquette S. *Anthropometric survey (ANSUR) II pilot study: methods and summary statistics*. Anthrotch, US Army Natick Soldier Research, Development and Engineering Center, 2009.
33. Pook L. P., F. Berto and A. Campagnolo. State of the art of corner point singularities under in-plane and out-of-plane loading. *Engineering Fracture Mechanics* 174: 2-9, 2017.
34. Ruan J., T. Khalil and A. I. King. Dynamic response of the human head to impact by three-dimensional finite element analysis. 1994.
35. Sahler C. S. and B. D. Greenwald. Traumatic brain injury in sports: a review. *Rehabilitation research and practice* 2012: 2012.
36. Salimi Jazi M., A. Rezaei, F. Azarmi, M. Ziejewski and G. Karami. Computational biomechanics of human brain with and without the inclusion of the body under different blast orientation. *Computer methods in biomechanics and biomedical engineering* 19: 1019-1031, 2016.
37. Shugar T. A. and M. G. Katona. Development of finite element head injury model. *Journal of the Engineering Mechanics Division* 101: 223-239, 1975.
38. Standring S. *Gray's anatomy e-book: the anatomical basis of clinical practice*. Elsevier Health Sciences, 2021.
39. Teo E. C., Q. H. Zhang and R. C. Huang. Finite element analysis of head–neck kinematics during motor vehicle accidents: Analysis in multiple planes. *Medical engineering & physics* 29: 54-60, 2007.
40. Thunnissen J., J. Wismans, C. Ewing and D. Thomas. Human volunteer head-neck response in frontal flexion: a new analysis. *SAE transactions* 3065-3086, 1995.
41. Thurston J. NCRP Report No. 160: ionizing radiation exposure of the population of the United States. IOP Publishing, 2010.
42. Trotta A. and A. N. Annaidh. Mechanical characterisation of human and porcine scalp tissue at dynamic strain rates. *Journal of the mechanical behavior of biomedical materials* 100: 103381, 2019.
43. Tse K. M., L. B. Tan, S. P. Lim and H. P. Lee. Conventional and complex modal analyses of a finite element model of human head and neck. *Computer methods in biomechanics and biomedical engineering* 18: 961-973, 2015.
44. Tse K. M., L. B. Tan, B. Yang, V. B. C. Tan and H. P. Lee. Effect of helmet liner systems and impact directions on severity of head injuries sustained in ballistic impacts: a finite element (FE) study. *Medical & biological engineering & computing* 55: 641-662, 2017.
45. Tuchtan L., Y. Godio-Raboutet, C. Delteil, G. Léonetti, M.-D. P. Marti and L. Thollon. Study of cerebrospinal injuries by force transmission secondary to mandibular impacts using a finite element model. *Forensic science international* 307: 110118, 2020.
46. Ungar O. J., U. Amit, O. Cavel, Y. Oron and O. Handzel. Age-dependent variations of scalp thickness in the area designated for a cochlear implant receiver stimulator. *Laryngoscope Investigative Otolaryngology* 3: 496-499, 2018.

47. Vasavada A. N., J. Danaraj and G. P. Siegmund. Head and neck anthropometry, vertebral geometry and neck strength in height-matched men and women. *Journal of biomechanics* 41: 114-121, 2008.
48. Wahid K. A., R. He, B. A. McDonald, B. M. Anderson, T. Salzillo, S. Mulder, J. Wang, C. S. Sharafi, L. A. McCoy and M. A. Naser. MRI Intensity Standardization Evaluation Design for Head and Neck Quantitative Imaging Applications. *MedRxiv* 2021.
49. Ward C. C. and R. B. Thompson. The development of a detailed finite element brain model. *SAE Transactions* 3238-3252, 1975.
50. Winter D. A. *Biomechanics and motor control of human movement*. John Wiley & Sons, 2009.
51. Winters J. M. Hill-based muscle models: a systems engineering perspective. In: *Multiple muscle systems*Springer, 1990, pp. 69-93.
52. Wu J. Z., C. S. Pan, B. M. Wimer and C. L. Rosen. Finite element simulations of the head–brain responses to the top impacts of a construction helmet: Effects of the neck and body mass. *Proceedings of the Institution of Mechanical Engineers, Part H: Journal of engineering in medicine* 231: 58-68, 2017.
53. Wu X., M. S. Downes, T. Goktekin and F. Tendick. Adaptive nonlinear finite elements for deformable body simulation using dynamic progressive meshes. In: *Computer Graphics Forum*Wiley Online Library, 2001, p. 349-358.
54. Zhang L., R. Makwana and S. Sharma. Brain response to primary blast wave using validated finite element models of human head and advanced combat helmet. *Frontiers in neurology* 4: 88, 2013.
55. Zhang L., K. H. Yang and A. I. King. A proposed injury threshold for mild traumatic brain injury. *J. Biomech. Eng.* 126: 226-236, 2004.
56. Zhang Q. H., E. C. Teo and H. W. Ng. Development and validation of a C0–C7 FE complex for biomechanical study. 2005.

Tables

TABLE 1. Material properties of each head-neck structure.

Segment	Material model	Material constants	Constitutive Equation
Scalp[27]	Linear viscoelastic	$G_0 = 1.70\ MPa, G_\infty = 0.68\ MPa$ $K = 20\ MPa$ $\beta = 0.00003$ $\rho = 1100\ kg/m^3$	$G(t) = G_\infty + (G_0 - G_\infty)e^{-\beta t}$
Skull[36]		$E = 15.00\ GPa$ $\rho = 1800\ kg/m^3$ $v = 0.21$	
Dura mater[45]	Linear elastic	$E = 5.00\ MPa$ $\rho = 1200\ kg/m^3$ $v = 0.45$	$\sigma = E\varepsilon$
Pia mater[45]		$E = 2.30\ GPa$ $\rho = 1000\ kg/m^3$ $v = 0.45$	
Vertebrae[43]	Linear elastic	$E = 8.00\ GPa$ $\rho = 1200\ kg/m^3$ $v = 0.22$	
CSF[7]	Hyper-elastic	$C_{10} = 0.0112$ $\rho = 1000\ kg/m^3$ $v = 0.499$	$W(J_1,J_2,J) = \sum_{p,q=0}^{n} C_{pq}(J_1-3)^p(J_2-3)^q + W_H(J)$
Brain[13]	Hyper-viscoelastic	$\mu = 0.014\ MPa, \alpha = 4.70$ $\rho = 1060\ kg/m^3$ $v = 0.45$ $K = 0.318\ MPa$ $G_1 = 0.099\ MPa, G_2 = 0.056\ MPa$ $\tau_1 = 0.008\ s, \tau_2 = 0.15\ s$	$W = \frac{\mu}{\alpha}(\bar{\lambda}_1^\alpha + \bar{\lambda}_2^\alpha + \bar{\lambda}_3^\alpha - 3) + \frac{K}{2}(J-1)^2$ $G(t) = \frac{\alpha \times \mu}{2} + \sum_{k=1}^{n} G_k exp^{-t/\tau_k}$
Intervertebral discs[5]	Hyper-viscoelastic	$C_{10} = 0.15, C_{01} = 0.03$ $\rho = 1000\ kg/m^3$ $v = 0.499$ $G_1 = 1.70, G_2 = 1.20, G_3 = 2.00$ $\tau_1 = 11.76, \tau_2 = 1.10, \tau_3 = 0.13$	$W(J_1,J_2,J) = \sum_{p,q=0}^{n} C_{pq}(J_1-3)^p(J_2-3)^q + W_H(J)$ $G(t) = \sum_{k=1}^{n} G_k exp^{-t/\tau_k}$
Muscles[30, 51]	Hill-type	PCSA[30] Muscle volume[30]	$F_{active} = F_{max} \times f_{FL} \times f_{FV} \times A(t)$ $F_{Passive} = \frac{F_{max}}{e^{K_{sh}} - 1}\left[e^{\frac{K_{sh}}{L_{max}}\left(\frac{L}{L_{rest}}-1\right)} - 1\right]\ For\ L > L_{rest}$
Ligaments[56]	Linear spring	k[56]	$F = kx$

E: Elastic modulus, G_0: short-term shear modulus, G_∞: long-term shear modulus, K: bulk modulus, β: decay constant, ρ: density, ν: Poisson ratio, τ_k: relaxation time, G_k: shear modulus, $\bar{\lambda}_i^\alpha$: principal stretch, W: strain energy density function, C_{pq}, μ, α: material constants, F_{active}: active muscle force, $F_{passive}$: passive muscle force, f_{FL} : force-length relation of the muscle, f_{FV}: force-velocity relation of the muscle, A(t): muscle's activation level versus time relationship, L_{rest} : the resting length and K_{sh} : passive muscle force constant, k: ligament stiffness.

TABLE 2. Geometrical comparison of the current model with the reported experimental values. F3, F4, T3, T4, P3, P4 are located at the frontal left, frontal right, temporal left, temporal right, parietal left, and right parietal regions of the skull, respectively.

Parameter	Reference	Model
Scalp thickness (mm)		
	Min: 3.0[2]	Min: 3.14
	Max: 14.2[2]	Max: 17.85
Skull thickness (mm)		
F3	5.95 ±1.40[20]	6.54± 1.43
F4	6.16 ±1.32[20]	5.51± 0.61
T3	3.31 ±0.80[20]	3.93± 0.19
T4	3.46 ±0.78[20]	3.15± 0.41
P3	6.36 ±1.30[20]	6.84± 0.55
P4	6.09 ±1.25[20]	5.76± 0.81
Brain volume (cm^3)	1173.33 - 1625.66[12]	1355.66
Cranial CSF volume (cm^3)	57.1 - 286.5[19]	305.851

TABLE 3 Cervical vertebrae measurements compared to experimentally reported values.

	Vertebral height (mm)		*Vertebral depth (mm)*		*Spinous process length (mm)*		*Vertebral body to spinous process length (mm)*	
	Model	*Vasavada et al.* [47]	*Model*	*Vasavada et al.* [47]	*Model*	*Vasavada et al.* [47]	*Model*	*Vasavada et al.* [47]
C2	-	-	-	-	20.18	20.9 ±3.5	38.09	35.8 ±3.6
C3	11.68 ±0.56*	13.5 ±0.7	15.47 ±0.56	14.2 ±1.6	19.64	18.8 ±2.4	33.02*	30.4 ±2.0
C4	13.47 ±0.46	12.6 ±0.8	14.53 ±1.47	14.8 ±1.2	26.76*	19.3 ±3.0	33.85*	30.1 ±2.8
C5	12.34 ±0.65	12.2 ±0.6	16.28 ±2.36	15.2 ±1.1	25.74	22.4 ±3.4	33.37	32.5 ±2.9
C6	11.93 ±1.70	12.0 ±0.7	19.42 ±1.41*	15.6 ±1.0	27.57	27.7 ±4.6	36.23	39.7 ±5.1
C7	12.41 ±2.23	13.0 ±1.0	18.73 ±0.67*	15.5 ±1.3	34.24	34.9 ±3.8	48.23	46.9 ±3.4

* Values outside one standard deviation of the literature.

TABLE 4. Angle-corrected, dimensionless intervertebral disc heights.

	Frobin et al.[14]	Model
C2/C3	0.346 ±0.067	0.303
C3/C4	0.382 ±0.077	0.366
C4/C5	0.393 ±0.059	0.375
C5/C6	0.381 ±0.042	0.295
C6/C7	0.363 ±0.056	0.323

TABLE 5. A Comparison between simulation results of Zhang et al. (non-injury cases), NBDL, and Nahum et al. studies and their corresponding experimental values.

Numerical simulations	parameters	Source	Value
Zhang et al.[55] study	Positive intracranial pressure (kPa)	Head-only model	57.96
		Head-neck model	26.28
		Reference	40 - 101
	Negative intracranial pressure (kPa)	Head-only model	44.36
		Head-neck model	19.00
		Reference	20 - 78
	Shear stress in midbrain (kPa)	Head-only model	7.58
		Head-neck model	2.48
		Reference	2.6-9.5
	Shear stress in thalamus (kPa)	Head-only model	4.27
		Head-neck model	2.25
		Reference	1.5-4.6
	Intracranial pressure peak time (ms)	Head-only model	10
		Head-neck model	24
		Reference	9
NBDL[40] study	Maximum neck angle (°)	Model	36.98 ±35.04 (maximum: 88.80)
		Experimental upper bound	39.70 ±33.54 (maximum: 87.50)
		Experimental lower bound	30.72 ±26.20 (maximum: 67.12)
	Peak time (ms)	Model	180
		Reference	175
Nahum et al.[29] study	Frontal intracranial pressure (kPa)	Head-only model	67.36 ±46.70 (maximum: 127.46)
		Head-neck model	65.54 ±30.46 (maximum: 123.93)
		Reference	75.56 ±42.74 (maximum: 141.19)
	Parietal intracranial pressure (kPa)	Head-only model	35.04 ±23.50 (maximum: 74.61)
		Head-neck model	20.60 ±11.68 (maximum: 57.83)
		Reference	41.06 ±22.09 (maximum: 73.59)
	Occipital intracranial pressure (kPa)	Head-only model	-28.57 ±13.56 (maximum: -43.28)
		Head-neck model	-25.44 ±15.14 (maximum: -69.01)
		Reference	-35.03 ±14.47 (maximum: -45.46)

Figures

Figure 1

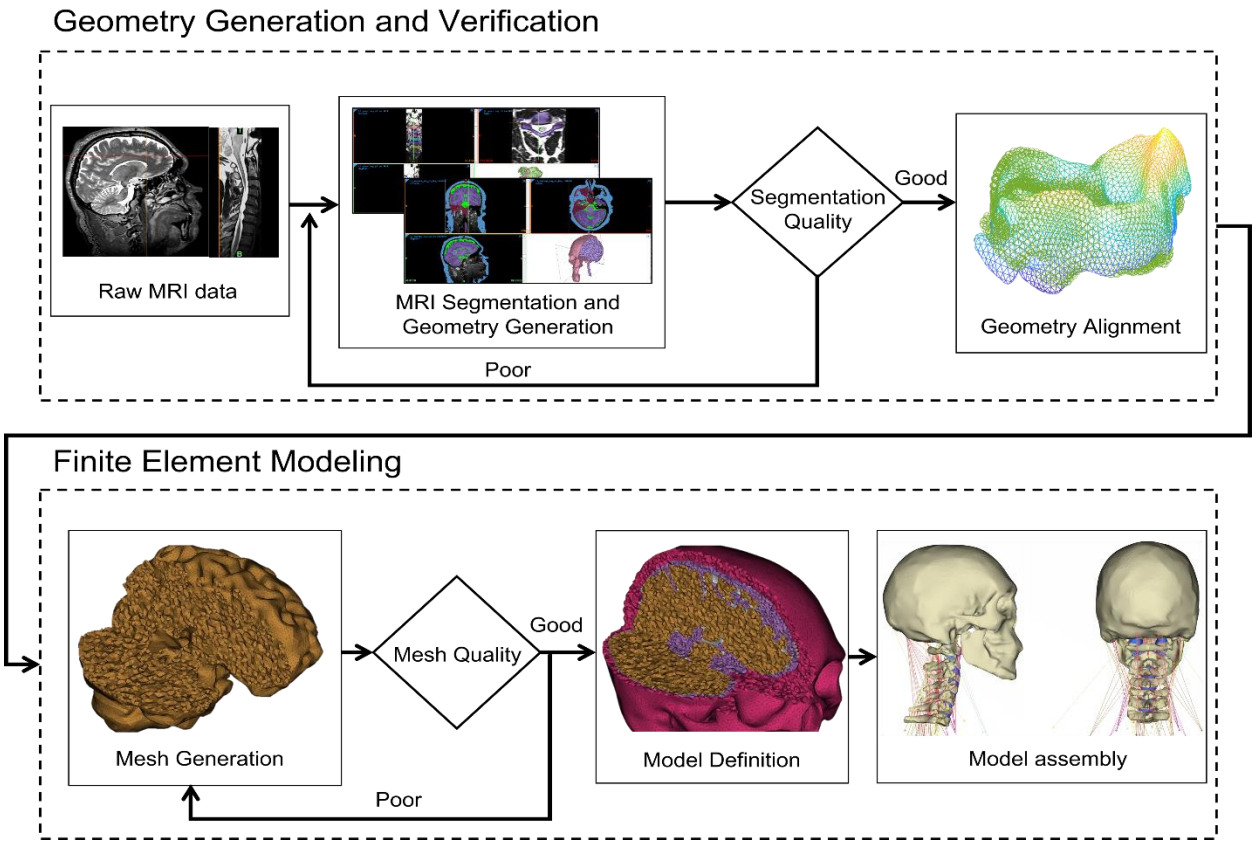

Figure 2

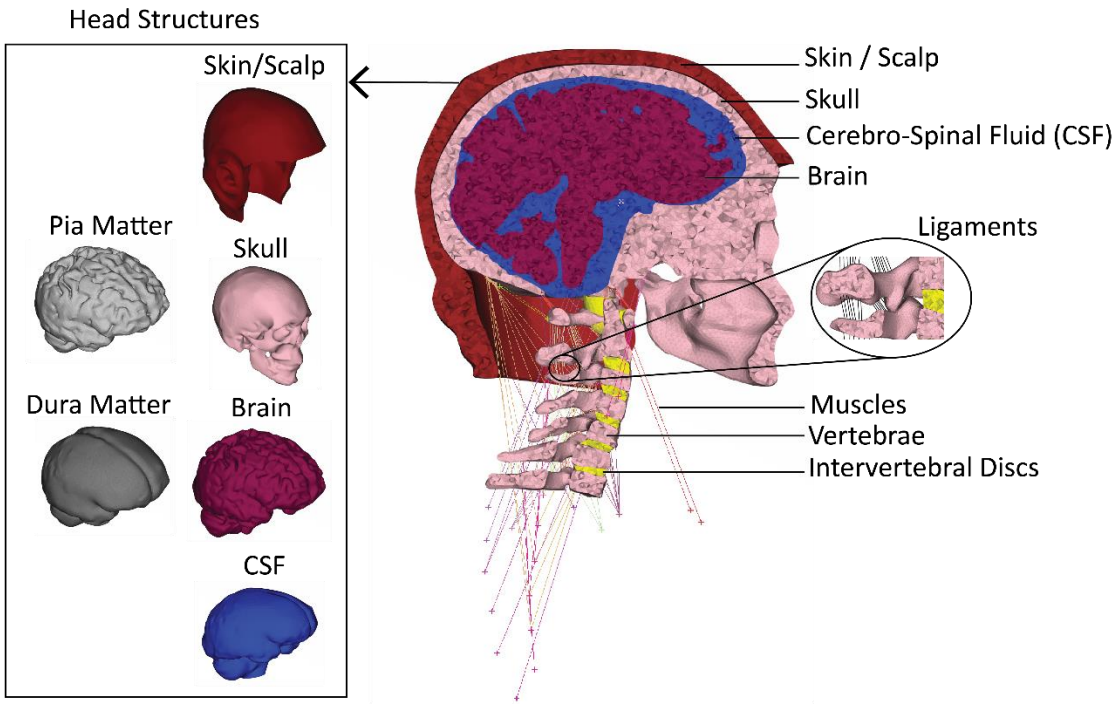
Head Structures
Skin/Scalp
Pia Matter
Skull
Dura Matter
Brain
CSF
Skin / Scalp
Skull
Cerebro-Spinal Fluid (CSF)
Brain
Ligaments
Muscles
Vertebrae
Intervertebral Discs

Figure 3

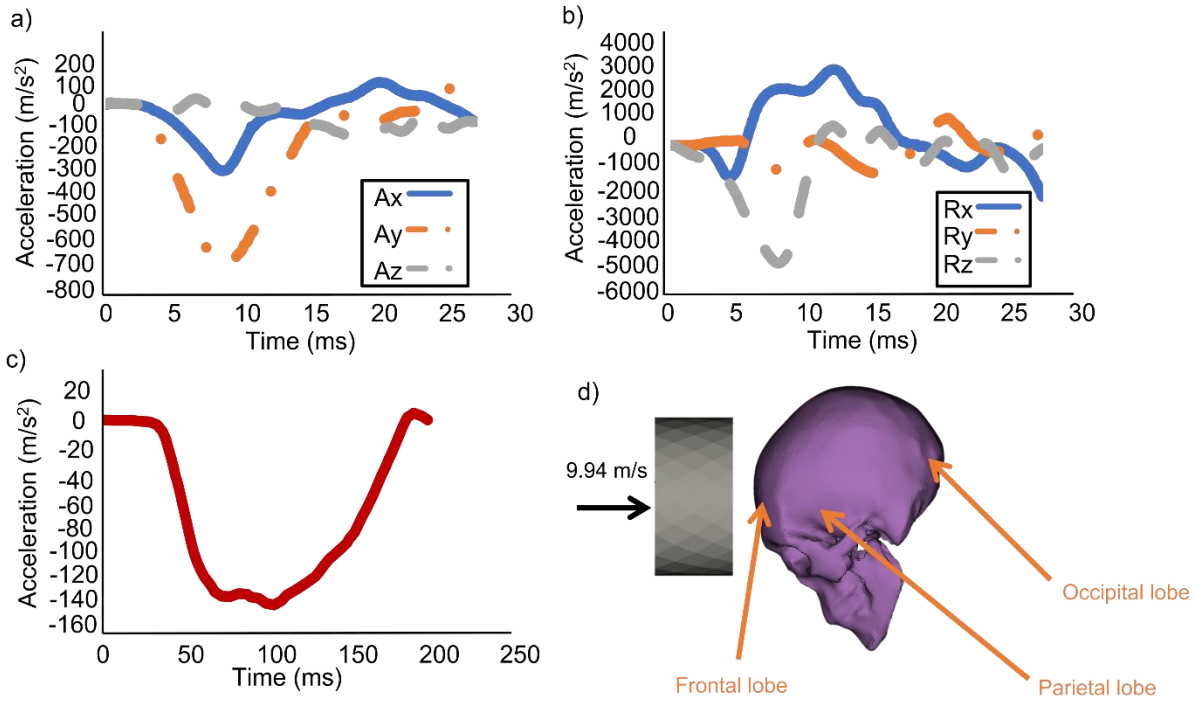
a)
Acceleration (m/s²)
200
100
0
-100
-200
-300
-400
-500
-600
-700
-800
0
5
10
15
20
25
30
Time (ms)
Ax
Ay
Az
b)
Acceleration (m/s²)
4000
3000
2000
1000
0
-1000
-2000
-3000
-4000
-5000
-6000
0
5
10
15
20
25
30
Time (ms)
Rx
Ry
Rz
c)
Acceleration (m/s²)
20
0
-20
-40
-60
-80
-100
-120
-140
-160
0
50
100
150
200
250
Time (ms)
d)
9.94 m/s
Occipital lobe
Frontal lobe
Parietal lobe

Figure 4

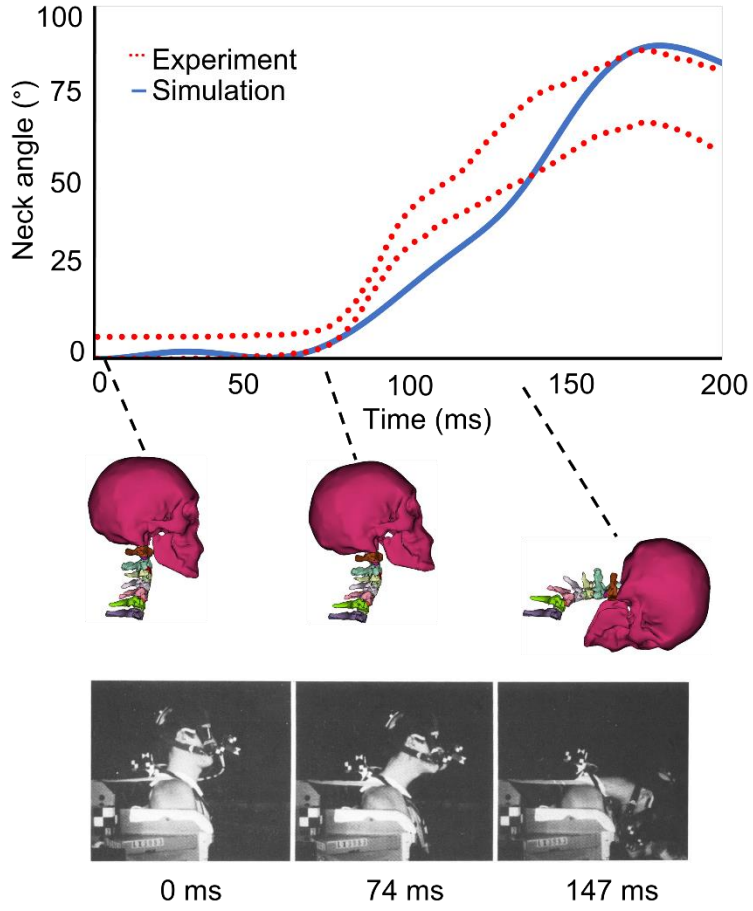
100
75
50
25
0
Neck angle (°)
Experiment
Simulation
0
50
100
150
200
Time (ms)
0 ms
74 ms
147 ms

Figure 5

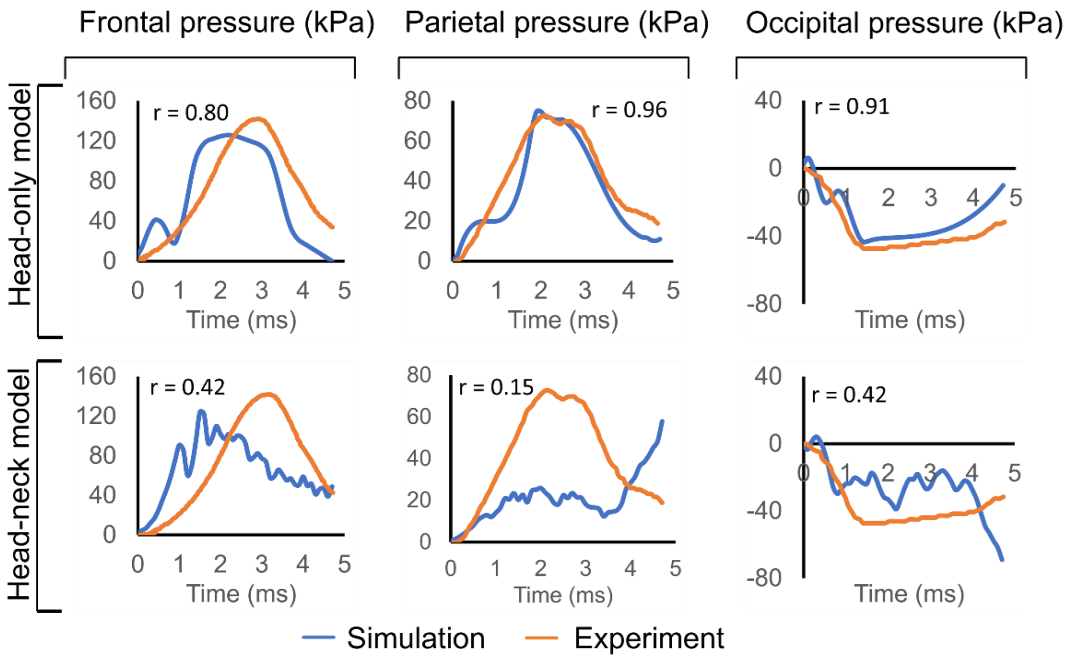
Frontal pressure (kPa)
Parietal pressure (kPa)
Occipital pressure (kPa)
Head-only model
Head-neck model
r = 0.80
r = 0.96
r = 0.91
r = 0.42
r = 0.15
r = 0.42
Time (ms)
Simulation
Experiment

Figure 6

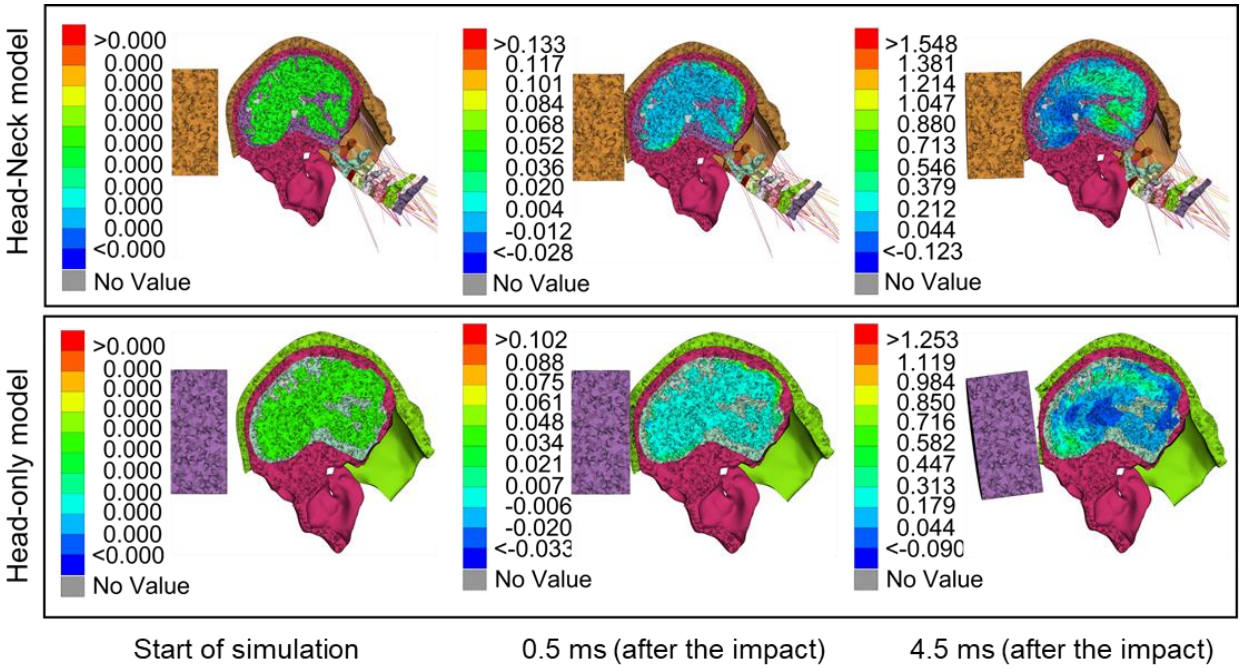
Head-Neck model
>0.000
0.000
0.000
0.000
0.000
0.000
0.000
0.000
0.000
0.000
<0.000
No Value
>0.133
0.117
0.101
0.084
0.068
0.052
0.036
0.020
0.004
-0.012
<-0.028
No Value
>1.548
1.381
1.214
1.047
0.880
0.713
0.546
0.379
0.212
0.044
<-0.123
No Value
Head-only model
>0.000
0.000
0.000
0.000
0.000
0.000
0.000
0.000
0.000
0.000
<0.000
No Value
>0.102
0.088
0.075
0.061
0.048
0.034
0.021
0.007
-0.006
-0.020
<-0.033
No Value
>1.253
1.119
0.984
0.850
0.716
0.582
0.447
0.313
0.179
0.044
<-0.090
No Value
Start of simulation
0.5 ms (after the impact)
4.5 ms (after the impact)